sustainability

MDPI

Article

Synthesis of Responsive Membranes for Water Recovery through Desalination of Saline Industrial Effluents

Elizabeth Vazquez [1], Claudia Muro [1,*], Sergio Pérez-Sicairos [2], Yolanda Alvarado [1], Vianney Díaz-Blancas [1] and Karina Hernández [1]

[1] Tecnológico Nacional de México, Instituto Tecnológico de Toluca, Avenida Tecnológico S/N Col, Metepec C.P. 52140, Mexico; evazquezr@toluca.tecnm.mx (E.V.); yalvaradop@toluca.tecnm.mx (Y.A.); vianney.db@toluca.tecnm.mx (V.D.-B.); khernandezg@toluca.tecnm.mx (K.H.)

[2] Departamento de Nanotecnología, Tecnológico Nacional de México, Instituto Tecnológico de Tijuana, Calzada Del Tecnológico S/N, Fraccionamiento Tomas Aquino, Tijuana C.P. 22414, Mexico; sergio.perez@tectijuana.edu.mx

* Correspondence: cmurou@toluca.tecnm.mx

Abstract: Polysulfone (PSF) and smart polymers (SRPs)—including polyacrylic acid (AAc), poly N-isopropylacrylamide (NIPA), and sulfonated poly(1,4-phenylene ether-ether-sulfone) (SPEES)—were used in the synthesis of responsive membranes (PSF-SRP) for application in sustainable desalination processes involving food industry effluents for water recovery and recycling. With the inclusion of SRPs, PSF-SRP membranes showed different characteristics when compared to the PSF membrane. AAc caused fibers to occur in the surface structure, increasing the MWCO of the PSF membrane, whereas NIPA and SPEES diminished the MWCO, resulting in ultrafiltration and nanofiltration membranes. Furthermore, NIPA and SPEES provided high mechanical and thermal resistance when incorporated into the PSF membrane. The performance of the membranes also showed important changes. In comparison with only PSF, PSF-SPEES and PSF-NIPA increased the water flux and salt rejection percentage by 20–30%. In addition, the highest membrane fouling resistance was observed with PSF-NIPA, while PSF-AAc and PSF-NIPA-AAc presented the lowest resistances. Therefore, PSF-NIPA and PSF-SPEES resulted in membrane improvement, including stimuli-responsive properties, allowing for effective saline effluent treatment.

Keywords: responsive membranes; desalination; water recovery; water recycling; industrial effluents; membrane fouling

Citation: Vazquez, E.; Muro, C.; Pérez-Sicairos, S.; Alvarado, Y.; Díaz-Blancas, V.; Hernández, K. Synthesis of Responsive Membranes for Water Recovery through Desalination of Saline Industrial Effluents. *Sustainability* **2024**, *16*, 5796. https://doi.org/10.3390/su16135796

Academic Editor: Andrea G. Capodaglio

Received: 19 April 2024
Revised: 13 June 2024
Accepted: 19 June 2024
Published: 8 July 2024

1. Introduction

Water recovery through industrial effluent treatment is a sustainable alternative for the production of reusable water. In particular, food saline industrial effluents provide an alternative drinking water source, contributing to the demand for clean water and addressing current water scarcity problems.

Saline water is mostly treated using membrane-based processes; however, membrane fouling is the principal restriction in terms of their productivity, leading to high costs associated with effluent treatment [1].

In order to address this issue, innovative polymers for membrane synthesis are being developed to increase the efficiency of membranes. Among them, materials named stimuli-responsive polymers (or smart/intelligent polymers; SRPs) are being studied for their potential use in the preparation of SRP membranes. SRPs are classified according to their effects on the membrane characteristics.

According to the physical and/or chemical properties of SRPs, they produce different membrane responses to various environmental stimuli, such as pH, temperature, polarity, light, and biological molecules, thus enhancing the permeation, fouling, lifetime, and

functionality aspects of membranes and consequently increasing their potential applications [2–5].

The most-studied SRPs include those in the polybenzimidazole (PBI), poly(N-isopropylacrylamide) (PNIPA), poly(poly (ethylene glycol), and poly(oligoethylene glycol (meth)acrylate) (PEGMA) families, as well as poly(acrylic acid) (PAAc), poly(methacrylic acids) (PMAs), poly(N-diethylaminoethyl methacrylate) (PDMA), and poly(ethyl pyrrolidine methacrylate) (PPMA) [6–8]. Other natural polymers, such as chitosan and cellulose, are also considered SRPs [9].

The preparation method for SRP membranes includes the blending of SRPs with a polymeric matrix, such as polyvinylidene fluoride (PVDF), polypropylene (PP), polyethylene (PE), polyamide (PA), polyethersulfone (PES), and/or polysulfone (PSF). Furthermore, surface membranes can be modified with SRPs, through covering a membrane or porous surface using coating and grafting processes. Detailed information on SRP membrane preparation methods can be found in the works of Saini et al. [7], Hou et al. [8], and Al-Najar et al. [9].

With the presence of SRPs, membranes acquire several stimuli-responsive properties, including changes in their pore size, charge, and transport properties.

The principal applications of SRP membranes are focused on ion exchange membranes for fuel cells, gas separation, energy storage, membrane electrodialysis, and food separation, including protein fractionation and concentration, and the clarification of juice, wine, and beer [10–12].

At present, water treatment is also an important topic, considering the progress of membrane systems that utilize SRPs as thermo-responsive and pH-responsive polymers [13]. Primary concerns in this context include the enhancement of hydrophilicity properties, chemical resistance to pH, oxidants, and chlorination. Nevertheless, the principal objective of SRP membranes is a reduction in membrane fouling [14]. Summarized reports containing details on the effect of the incorporation of pH-responsive polymers can be found in the work of Al-Najar et al. [9]. Furthermore, Musarurwa and Tavengwa [15] have referred to the achievement of reversible properties; namely, hydrophilicity and antifouling capacity.

Experimental reports on SRP membrane applications include the work of Choi et al. [16], who developed a PES membrane with high enhancement in relation to the flux and fouling properties through blending poly(2-dimethylaminoethyl methacrylate)-block-poly(N-isopropylacrylamide) with (PDMAEMA-b-PNIPAM, PDN). Liu et al. [17] grafted a thin PA film with acidic aqueous glutaraldehyde and monomethoxy-poly(ethylene glycol) (MPEG) to produce a membrane for textile dye separation and to enhance the durability and susceptibility of PA to chlorine.

Chen et al. [18] fabricated a membrane made of PA, incorporating an aliphatic diamine of 1,3-diamino-2-propanol (DAPL) and grafting PVA on the top surface of the DAPL-based PA layer to enhance its hydrophilicity. Ghassemi et al. [19] developed a dual-functionalized PES membrane, which involved grafting with NIPA and subsequent functionalization with copper oxide nanoparticles, in order to improve the membrane flux and fouling properties.

SRP membrane development has also recently been considered in terms of desalinization purposes. Hu et al. [20] grafted dialdehyde carboxymethyl cellulose (DACMC) onto the surface of a nascent PA, increasing the hydrophilicity, surface smoothness, and NaCl retention. Lü et al. [21] modified a PA-based thin-film composite membrane through grafting polyethyleneimine (PEI) onto the surface of the base membrane at the sites of the carboxylic groups, enhancing the $CaCl_2$/NaCl rejection ratio and the resistance to deposition by both cationic and anionic dyes. Li et al. [22] prepared an SRP membrane through interfacial polymerization of PA on a PE-based porous membrane, improving its hydrophilicity and NaCl separation ability. Similarly, Zhao et al. [23] synthesized PA membranes with UiO-66-NH_2 nanoparticles embedded on a hydrophobic PES surface, using a heterogeneous surface regulated interfacial polymerization approach for high-performance desalination and wastewater treatment applications.

According to the latest data, the fabrication of responsive membrane systems using SRPs remains a topic of interest in the context of separation processes to enhance the functionality of membranes. However, there are still some challenges, including the long-term stability of SRP under external stimuli, optimal composition of SRPs in matrices, mechanical resistance of SRP membranes during their operation, new anti-fouling membranes for use in different applications, and evidence of the effectiveness of SRP membranes in complex effluents. Therefore, more studies are necessary to contribute to the knowledge on membranes for the treatment of industrial effluents, wastewater treatment, and separation processes.

The aim of this work was the development of PSF-SRP membranes that are responsive to certain stimuli through the incorporation of polyacrylic acid (AAc), poly N-isopropylacrylamide (NIPA), and sulfonated poly(1,4-phenylene ether-ether-sulfone) (SPEES) as SRP materials to generate membranes with high water permeability and antifouling behavior under inorganic fouling. The synthesis of responsive membranes is carried out with the purpose of providing a specific application for the sustainable processing of wastewater for recovery from saline industrial effluents.

2. Materials and Methods

2.1. Materials and Reagents

Polysulfone (PSF), polyacrylic acid (AAc, 99%, 100,000 g/mol), poly N-isopropylacrylamide (NIPA, 98%), poly(vinylidene fluoride) beads (PVDF), poly(1,4-phenylene ether-ether-sulfone) pellets (PEES), dichloromethane-methanol-water (DMW), dimethylformamide $\geq$ 99% (DMF), dextran T1000 (1 kDa), dextran T5000 (5 kDa), dextran T10,000 (10 kDa), and dextran T100,000 (100 kDa) were obtained from Sigma-Aldrich, Burlington, MA, USA. Phosphate buffer stock solution (Thermo Scientific, Waltham, MA, USA), deionized water (DI), and distilled water were obtained using a Millipore Direct-Q water purification system (Burlington, MA, USA). The saline wastewater effluent was provided by the food industry.

2.2. Membrane Manufacture

PSF was used as a polymeric matrix, while the SRP agents were NIPA (a thermoresponsive polymer), AAc (a pH-responsive polymer), and SPEES (an ionic polymer). The casting solutions were synthesized through in situ cross-linked polymerization of NIPA, AAc, and SPEES in PSF solutions.

The sulfonation of PEES was previously carried out by the dissolution of 5 g of PEES in 130 mL of H_2SO_4 (0.4 M sulfonating agent) with mechanical agitation (400 rpm) for 64 h at room temperature [24]. The solution was precipitated in ice-cold DMW and decanted to obtain sulfonated PEES (SPEES). SPEES was washed with DMW until a pH range of 6–7 was achieved. The SPEES product was dried for 12 h at 60 °C, and then kept at room temperature.

For membrane preparation, polymeric solutions were prepared by dissolving different proportions of PSF (polymeric matrix) and SRP agents (i.e., AAc, NIPA, and SPEES) in dimethylformamide (DMF) as solvent. Dissolutions were carried out in a rotary device with intermittent stirring (40 rpm) under a heating lamp at 70 °C, in order to promote dissolution of the polymers.

Table 1 shows the used percentages of PSF, SRP agents, and DMF in the preparation of casting membrane solutions. The data also include those for the composition of PSF membrane without any SRP. In this case, the PSF membrane was used as a blank to determine the effects of the SRPs in PSF. Furthermore, a polyvinylidene difluoride (PVDF) membrane was also prepared, which was used as membrane control according to its known hydrophobic, high mechanical resistance, and thermal stability properties.

Table 1. Composition (% *w*/*w*) of casting solutions for preparation of SRP membranes.

Membrane	PSF	NIPA	AAc	SPEES	DMF
PSF	21	0	0	0	79
PSF-AAc	18	0	3	0	79
PSF-NIPA	18	3	0	0	79
PSF-NIPA-AAc	15	3	3	0	79
PSF-SPEES	19	0	0	2	79
PVDF	21	0	0	0	79

All membranes were obtained using the phase inversion method, using a molding machine with a Holitex 3329 support material and knife (model 22LN30, acquired from the company P3 Srl, Padua, Italy). Polymeric solutions were cast onto Holitex support. The knife was used with a dispersion opening of 0.015 mm. According to previous experiments, the immersion speed was 80 rpm (5 m/s) and the temperature was 25 °C.

Subsequently, the immersion phase was carried out in a water bath at a temperature of 20 °C. Finally, the flat membrane was removed from the equipment and rinsed three times for two minutes with deionized water to eliminate the remaining solvent that might have been trapped in the porous membrane and to remove the excess floating polymer. Clean membranes were then stored in deionized water and refrigerated.

2.3. Membrane Characterization

Dry samples of PSF-SRP membranes (0.4 × 3.5 cm) were characterized according to the following parameters.

1. Superficial morphology analysis using JEOL scanning electron microscopy (SEM) (JSM 5300). This study was carried out through deposition of a thin layer of gold on the surface of each membrane sample using a Technic Hummer 5 sputter-coated evaporator.
2. Membrane thickness analysis using a Mitutoyo Absolute caliper. Thickness was measured in dry membranes, and indicated in mm.
3. Pore characteristics assessed through the BET technique, using nitrogen for gas adsorption analysis.
4. Membrane porosity percentage (MP%). The membranes were brought to constant weight, registering the data (W1). Then, the membranes were submerged in deionized water for two days. Subsequently, they were dried at 100 °C for 1 h and placed in a desiccator to cool to room temperature. The dried membranes were weighed again to achieve constant weight (W2). The percentage of water absorbed by each sample was calculated using Equation (1), which includes the membrane volume (Mv) and water density (wρ).

$$\mathrm{MP\%} = \frac{\mathrm{W1} - \mathrm{W2}}{(\mathrm{Mv})(\mathrm{w}\rho)} \times 100 \quad (1)$$

5. Membrane hydration according to water retaining percentage (MH%). The dry membrane (Wd) samples were weighed up to constant weight. Subsequently, the membranes were placed in deionized water for 5 h. The wet weight (Ww) was recorded, and water retention results were obtained using Equation (2). In addition, the swelling thickness due to MS was measured using a Mitutoyo Absolute caliper.

$$\mathrm{MH\%} = \frac{\mathrm{W_w} - \mathrm{W_d}}{\mathrm{Ww}} \times 100 \quad (2)$$

6. Membrane hydrophilicity was measured by means of water contact angle analysis, using a goniometer equipped with Pinnacle Studio HD v15.0 video control software and Ramé-Hart Instrument Co. controlled drip dispenser from IIM. The procedure

was based on the ASTM D 2578-04, ASTM C 813-90, and ASTM D 5946-99 standards [25–27]. To carry out determination, 3 membrane samples of approximately 1.5 cm^2 were glued onto 2 × 3 cm acrylic supports and were later compressed to obtain a flat surface. The measurement was carried out at room temperature, proceeded in triplicate by adding a 4 µL drop of tri-distilled water at 3 different points on the surface of each membrane, and videotaped for 20 s.

7. Surface charge density was assessed using a titration method. The surface of each membrane was treated with a 1 M HCl solution, in order to replace the mobile counterions with H+. Then, the membranes were washed with deionized water until they reached a neutral pH. The membrane was placed in contact with a solution of 0.1 M NaOH for 2 min. Next, 20 mL of the contact solution was titrated with a 0.1 M aqueous HCl solution, using a 1% phenolphthalein solution as indicator. The charge density on the membrane surface was calculated as the difference between the meq of the NaOH solution before and after it was neutralized. The result is reported in meq of Na^+/m^2.
8. Thermal Stability Profile (TGA) was analyzed using a TA Instruments Model SDT 2960 thermogravimetric analyzer, starting from room temperature up to 800 °C, at a heating rate of 10 °C per minute.
9. Mechanical behavior patterns were assessed using a TA Instruments model Q800 mechanical dynamic analyzer. Samples were analyzed with a size area of 0.4 × 3.5 cm.

2.4. Membrane Performance

Performance tests were carried out on a cross-flow filtration system. Figure 1 shows the filtration system, using a flat membrane module, containing a flat membrane with an effective filtration area (A) of 18 cm^2.

Figure 1. Cross-flow filtration system of flat membrane module, used for performance evaluation of PSF-SRP membranes.

The filtration system consisted of a housing of flat membranes connected by pipes with two manometers and valvules, one placed on the feeding side and the other on the permeate side of the membrane. Both manometers provide the inlet and outlet pressure values of the membrane. The transmembrane pressure (TMP) is measured as an average of the two pressures, measured on the supply side in the range of 0–10 bar.

The following tests were conducted to determine the membrane performance; each test was performed in triplicate.

1. Rejection test of dextran for determination of experimental molecular weight cut-off (MWCO) of the membranes. The dextran rejection of the PSF-SRP membranes was assessed to evaluate the experimental MWCO of the membranes, the retention capacity, and the predominant large pore size of the membranes.

Dextran mixture was prepared at different molecular weights (MWs; 1, 5, and 10 kDa) using 1% dextran, according to the theoretical MWCO of membranes. The dextran was dissolved in a buffer at pH 7.5, using phosphate buffer stock solution.

PSF-SRP membranes were fed with dextran at room temperature in recycle mode to measure the retention percentage of dextran [28]. The experiments were carried out at a TMP of 8 bar and room temperature for 90 min. A volume of 20 mL of membrane permeate and rejection were collected, in order to determine the content of saccharides in dextran using an ATAGO N-10 refractometer. Equation (3) was used to calculate the rejection percentage of dextran particles (DR%), with Cf denoting the concentration of dextran in the feed and Cp denoting the concentration of dextran in the permeate.

$$DR\% = 1 - \frac{Cp}{Cf} \tag{3}$$

2. Water flux permeates under different operating conditions for the PSF-SRP membranes and PVDF membrane control, including (a) TMP variation (2–8 bar) to determine the maximum pressure and feed pressure range. The membranes were fed with distilled water at room temperature (20–25 °C). (b) Feed temperature variation, in order to determine the optimal range of feed temperatures for the membranes. Distilled water was fed in a temperature range of 20–40 °C at pH 6.6. (c) The feed pH range was determined through feeding distilled water at pH 4–8 at room temperature with TMP of 8 bar. The range of operation conditions was determined according to the water flux permeate Jp (mL/scm^2) using Equation (4), considering the volumetric flux Qp (mL/s) and membrane area A (cm^2).

$$Jp = \frac{Qp}{A} \tag{4}$$

3. The salt rejection percentage (%) of PSF-SRP membranes was measured during the treatment of a brackish industrial effluent from the food industry, containing 10,000–20,000 of total dissolved solids (TDS) equivalent to salts, in the conductivity range of 14–28 mS/cm at pH 8 and 25 °C. The salt rejection % was calculated from the volume of rejection from permeation source per unit of time, using a similar equation to (3), with salts as the solute.

4. Membrane resistance to fouling was assessed according to the sum of hydraulic membrane resistance (HR) and resistances due to fouling (FR), including reversible fouling resistance (RFR) and irreversible fouling resistance (IFR).

TR was measured according to the permeate flux at membrane saturation when the flux was reduced, during the treatment of brackish industrial effluent from the food industry. Equation (5) describes the TR and Equation (6) designates the FR.

In turn, HR describes the water flux (Jw) of the membrane without the presence of fouling (clean membrane), supplying the membrane with distilled water at TMP and taking the viscosity (μ) of water into consideration. Equation (7) defines the HR.

$$TR = HR + FR = \frac{TMP}{\mu Jp} \tag{5}$$

$$FR = RFR + IFR \tag{6}$$

$$HR = \frac{TMP}{\mu Jw} \tag{7}$$

Equation (8) was used to calculate the RFR, where J is the flux from the membrane after its use and the removal of reversible fouling through the washing of the membrane, while the IFR was calculated using Equation (9) [29,30].

$$RFR = \frac{TMP}{\mu J} \tag{8}$$

$$IFR = TR - RFR - HR \tag{9}$$

3. Results and Discussion

3.1. Morphological Characteristics of PSF-SRP Membranes

Figure 2 shows SEM images of membranes manufactured using the phase inversion method, including PSF, PSF-SRP, and PVDF membranes (the latter as control).

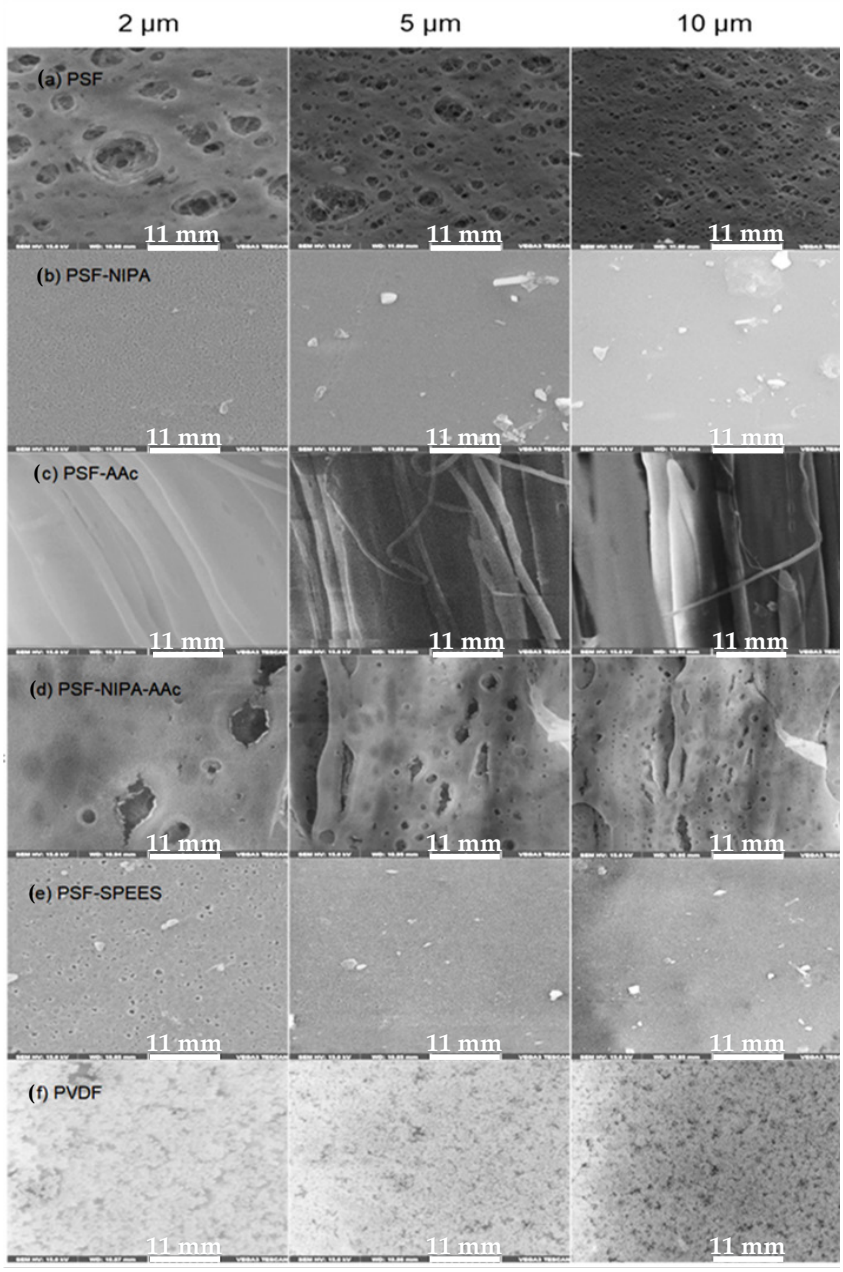

Figure 2. Microscopic images of membranes manufactured using phase inversion method, including PSF membrane, PSF-SRP membranes, and PVDF membrane (control) (2, 5, and 10 µm of magnification).

The images show the pore structure of the PSF membrane, exhibiting a surface with slight irregularity and larger pores in comparison with the membranes including SRPs. Specifically, the PSF membrane was confirmed to possess a fully sponge-like structure and smooth top surface with conspicuous pores [24]. The PSF pores and surface structure are associated with the characteristics of the polymer and membrane preparation conditions such as the viscosity and precipitation rate of the polymer solution [31]. Similarly, images of the PVDF membrane control present its well-known structure, showing smaller pores and regular porosity [32].

In turn, the microscopic images reveal the alterations in the pore and surface structure of PSF membranes with the presence of SRPs. Specifically, the incorporation of NIPA and SPEES in PSF produced membranes with reduced pores, as well as smooth and homogeneous surfaces.

In contrast, the incorporation of AAc produced striations on the PSF surface and irregular pores in PSF-AAC and PSF-NIPA-AAc membranes, presenting a fibrous surface with spaces between the fibers of micrometric sizes; meanwhile, NIPA in PSF-NIPA-AAc enhanced the membrane surface, with the evident formation of pores. Nevertheless, fibers and macro voids can also be observed in these membranes, which are due to the presence of AAc. The surface characteristics caused by the presence of AAc were attributed to the concentration and viscosity of AAc, as well as temperature conditions of membrane preparation.

Luo et al. [33] observed that the inclusion of AAc in PES membranes produced a structure with finger-like macro voids beneath a skin. However, Plisko et al. [34] found that AAc can expose different structures in a manner dependent on its concentration and MW. Similarly, diminishing of the rate of the solvent during phase separation also affects the membrane surface morphology.

Regarding NIPA and SPEES, Zhu et al. [30] and Manohar et al. [35] showed that the introduction of NIPA into the PSF membrane surfaces and pore walls produced a membrane with bi-continuous nanopores throughout its whole thickness, whereas SPEES leads to membrane surfaces with dense and homogenous nature without any cracks and holes.

Other results from SPR blending in membranes have been reported by Zhao et al. [29], who included hydrophobic layers of PES and embedded nanoparticles into pristine PA membranes, leading to different smoother and thinner PA layers and diverse structures in a manner dependent on the interfacial polymerization conditions during membrane preparation. However, factors such as the matrix of modification, SRP characteristics, the insertion method of SRP, the solvent, viscosity of the polymer, and conditions of membrane preparation have significant influences on the membrane structure. Zhu et al. [36] revealed that in situ cross-linking of AAc into PSF produced decreasing pore size with exposure time increasing from 0 to 60 s. Peng et al. [37] also studied the effect of exposure time on PVDF, showing alterations in the formation of pores with changes in the exposure time.

3.2. Surface Characteristics of PSF-SRP Membranes

Table 2 exposes the characteristics of PSF-SRP membranes, as well as the control (PVDF) membrane. The data indicate that the presence of SRPs in PSF altered the membrane surface characteristics, depending on the SRP, as described below.

Table 2. Surface characteristics of PSF-SRP membranes.

PSF-SRP Membrane/Characteristics	PSF	PSF-AAc	PSF-NIPA	PSF-NIPA-AAc	PSF-SPEES	PVDF
Thickness (μm)	145	182	140	165	140	140
Pore radius (μm)	0.10	ND *	0.010	0.10	0.050	0.020
Membrane porosity (MP%)	60	15	80	55	70	75
Hydrophilicity Contact angle (°) at 25 °C	65	60	60	55	62	80
Membrane hydration (MH%)	28	48	30	43	31	15
Swelling thickness (μm)	3	6	4	5	4	2
Surface charge densities (SCD meq Na+/m^2)	120.8	213.3	123.5	134.1	179.2	148.2

* Not detectable measurement.

1. Membrane thickness. The equipment and the phase inversion condition in the manufacturing of membranes produced membranes with similar thickness (140–145 μm); however, PSF-AAc and PSF-NIPA-AAc membranes showed differences in pore size. The

differences were associated with the incorporation and viscosity characteristics of AAc in PSF, as the conditions of the preparations were analogous.

2. Pore radius. The PSF-SRP membranes showed different pore sizes; PSF showed 0.10 µm, while the PVDF membrane control showed 0.020 µm. Nevertheless, the presence of NIPA and SPEES in PSF reduced the pore radius, achieving an average of 0.010–0.050 µm.

PSF-NIPA-AAc also showed an alteration in the porous radius with the predominant influence of AAc, causing irregular pores and macro voids. In turn, BET analysis of PSF-AAc showed that nitrogen was not retained by the pores, indicating scarce pore formation. Therefore, the pore radius was not detected (ND*). In this case, the pore radius results in PSF-SRP membranes were linked to the characteristics of the SRPs and, particularly, to the preparation conditions of PSF-AAc.

3. Membrane porosity (MP%). The MP% of PSF was modified with the incorporation of SRPs. Specifically, the presence of NIPA and SPEES increased the MP%, in comparison to PSF; meanwhile, PSF-NIPA-AAc decreased the MP%. In particular, PSF-AAc showed low MP%, as the presence of AAc formed fibers on PSF, causing channels and low porosity in the membrane (according to the SEM images and pore radius results). In turn, the PVDF membrane showed high porosity [37].

The MP% data were linked with the conditions of membrane preparation. Harruddin et al. [38] found that PES-DMAC membranes suffered changes in MP% in a manner dependent on the exposure time of polymer to the solvent, in particular, increasing along with the exposure time due to the increasing interconnection of the cellular pores, as the polymer solution had sufficient time to crystallize and produce pores in the membrane. However, data on PSF-NIPA, PSF-SPEES, PSF-AAc, and PSF-NIPA-Aac were not found in the literature.

4. Membrane hydration (MH%). The MH% in PSF-SRP membranes was also modified, indicating that AAc, NIPA, and SPEES changed the number of chemical groups interacting with water in PSF, which resulted in a change in the water adsorption ability.

The high water retention in PSF-AAc and PSF-NIPA-AAc membranes was associated with membrane fibers and asymmetric porousness. However, the properties of NIPA and AAc also can produce positive alterations in the membrane, as NIPA is a thermo-responsive polymer that regulates the hydrophilicity of the membrane surface, while AAc is a pH-responsive polymer, acting in dependency with the pH.

Due to deprotonation, AAc alters the osmotic pressure and hydration, resulting in high water retention. However, Junker et al. [39] modified PES membranes with poly(allylamine hydrochloric acid) (PAH) and AAc, and revealed the strong effects of pH. High swelling and water permeability were detected at pH 9, while a decrease in MWCO at pH 9 was also observed. This result was linked with the excess charge due to the presence of PAH and AAc.

Water retention under the introduction of a thermo-responsive polymer into membranes has also been analyzed by Choi et al. [16], who showed that the membrane hydration ability of PES can be enhanced in the presence of poly(2-dimethylaminoethylmethacrylate)-block-poly(N-isopropylacrylamide) (DMAEMA-b-NIPAM), due to alterations in its pore structure and membrane hydration.

5. Hydrophilicity of PSF-SRP membranes. According to the blend of AAc, NIPA, and SPEES in PSF for membrane preparation, the hydrophilicity property presented a notable increment, which was observed in accordance with the contact angle decreasing in PSF-NIPA, PSF-SPEES, and PSF-NIPA-AAc membranes, showing a 5–10% contact angle reduction with respect to the original PSF. PSF-NIPA-AAc presented principal reduction of the contact angle due to the presence of both AAc and NIPA, as both provide hydrophilic properties.

Plisko et al. [34] showed that more efficient hydrophilization of the PSF membrane surface was enabled with the addition of 0.4 wt% of AAc at 450,000 g/mol of MW, reducing the water contact angle from 65° in pristine PSF to 19° in PSF-AAc. The angle reduction was attributed to the quantity of highly hydrophilic carboxylic groups provided by AAc. Zhu et al. [24] synthesized PSF membranes by copolymerizing AAc and vinyltriethoxysilane

(VTEOS) in PSF solution and observed that AAc was more effective in improving membrane hydrophilicity, whereas VTEOS improved membrane stability.

The effect of NIPA on the water contact angle in SRP membranes has been reported by Ghassemi et al. [19]. In this case, the authors evidenced the thermo-responsive characteristics of NIPA, substantially enhancing the hydrophilicity of the PES membrane.

6. Surface charge densities (SCDs) of membranes. According to the data in Table 2, the presence of AAc and SPEES increased the negative charge, which is linked with their polyelectrolyte nature [40–44]. In contrast, it was observed that the PSF-NIPA membrane showed a lower SCD than the original one; this is because NIPA has neutral charge, leading to a small change in SCD in PSF-NIPA and PSF-NIPA-AAc.

Other SPRs have also been tested to change the surface charge of membranes. Wang et al. [43] improved the positive surface charge through the inclusion of poly(methyl methacrylate-co-dimethyl aminoethyl methacrylate) (P(MMA-co-DMAEMA)) in PSF. The authors detected that the addition of charge led to increments in hydrophilicity and fouling resistance.

3.3. Thermogravimetric Analysis of PSF-SRP Membranes

Figure 3 shows the thermograms of PSF-SRP membranes, including ramps from 0 to 800 °C. The thermal stability behavior of the PSF membrane was improved with the presence of the SRPs. The first loss of water, solvent, and sulfonic groups was observed in PSF and PVDF membranes at 378 °C and 447 °C, respectively, whereas PSF-AAc, PSF-SPEES, PSF-NIPA-Aac, and PSF-NIPA membranes showed increments in thermal stability (488–505 °C). In turn, a weight reduction of 50% was observed in the PSF membrane at 482 °C, followed by PSF-SRP (551–587 °C) and PVDF (620 °C), with the highest thermic stability offered by PSF-NIPA. However, the PVDF control presented a degradation temperature (Td) of 448 °C with 27% of weight residue, whereas PSF and PSF-SPEES membranes were degraded at 498 °C with 44% of weight residue. The range of Td in PSF-NIPA, PSF-AAc, and PSF-NIPA-AAc membranes was 503–507 °C with residues of 35–39%, confirming that NIPA provided the highest thermic stability when added to PSF.

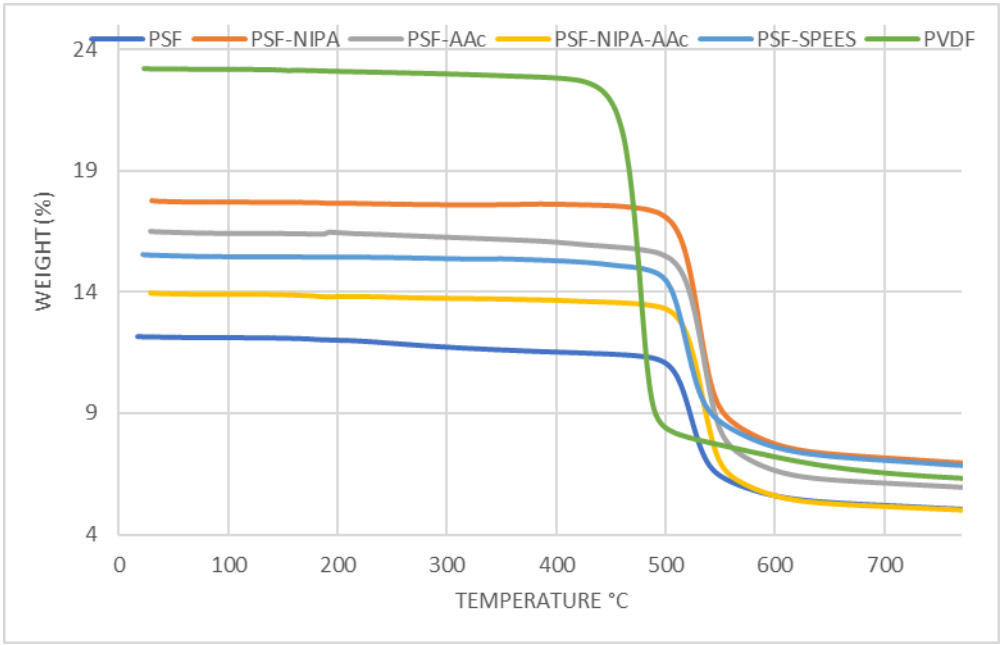

Figure 3. Thermograms of PSF, PSF-SRP, and PVDF membranes.

The thermal capacity of NIPA has been stated in several reports. Ghassemi et al. [19] grafted PES membranes using NIPA, AAc, and nanoparticles of CuO. As a result, the modified PES membranes showed higher thermal stability, compared to the sole PES.

3.4. Dynamical Analysis of PSF-SRP Membranes

Figure 4 depicts the dynamic mechanical analysis (DMA), exhibiting data on the deformation at rupture (strain %) of PSF-SRP membranes and their mechanical responses as tensile stress (TS) in units of MPa.

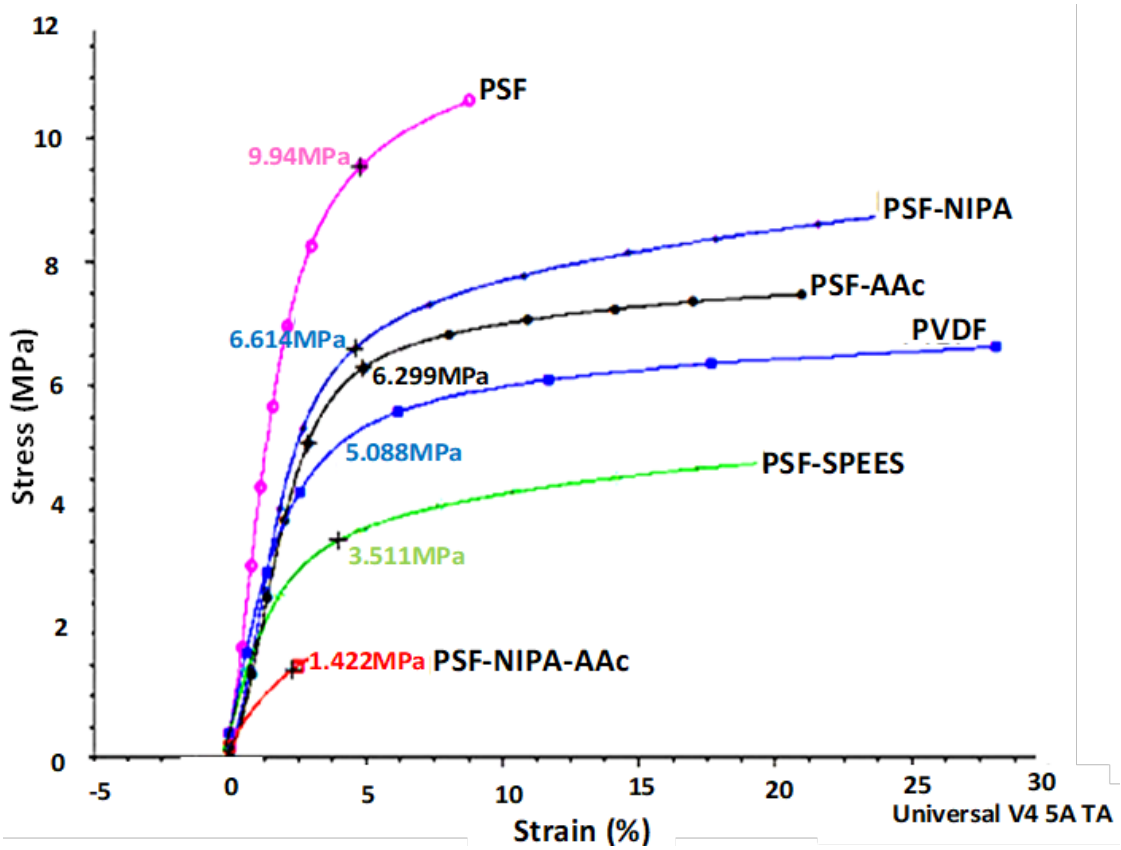

Figure 4. Dynamic mechanical analysis (DMA) curves of PSF-SRP membranes, as well as PVDF membrane (control).

The PSF membrane showed a higher TS than the other membranes, indicating high mechanical resistance and maximum elongation, due to its plasticizing effect. This means that the PSF membrane has intrachain spaces, allowing for high elongation and low stiffness (Young modulus); however, this behavior was detected in a short range of deformation (strain%), compared to the PSF-SRP membranes. Sequentially, the TS% behavior of PSF-SRP membranes was as follows: PSF > PSF-NIPA > PSF-AAc > PVDF > PSF-SPEES in wide ranges of strain %, suggesting lower elongation than the PSF membrane, but with high deformation range, thus enhancing the Young modulus. The high TS in PSF-NIPA was congruent with its characteristics of shrinking retractable elastic deformation, comparable to that of PVDF. However, a different behavior was observed in PSF-NIPA-AAc; here, the membrane reduced 85% of TS value within a short range of deformation, in contrast to PSF and the other PSF-SRP membranes. In this case, the membrane's mechanical properties were attributed to change in pore structures due to the presence of AAc.

An increase in the mechanical stability of membranes with the introduction of SRP has also been reported by Beshahwored et al. [44], who tested the inclusion of polybenzimidazole (PBI) into sulfonated polyphenylsulfone (sPPSU), enhancing the mechanical stability by 10%. Zhu et al. [31] synthesized antifouling PSF membranes through copolymerization

of AAc and vinyltriethoxysilane (VTEOS) in PSF solution. The authors observed that AAc was more effective in terms of membrane hydrophilicity improvement, whereas VTEOS elevated the membrane stability. In turn, according to Khan et al. [45], the presence of SPEES provided high mechanical properties in carbon nanotubes (SWNT).

3.5. Performance Evaluation of PSF-SRP Membranes

1. The rejection percentage of membranes was determined according to the filtration of polymer molecules of dextran at different MWs for experimental determination of MWCO membranes and membrane pore distribution.

Figure 5 shows the dextran retention percentage (DR%) and pore size distribution data for the PSF-SRP membranes and PVDF membrane (control).

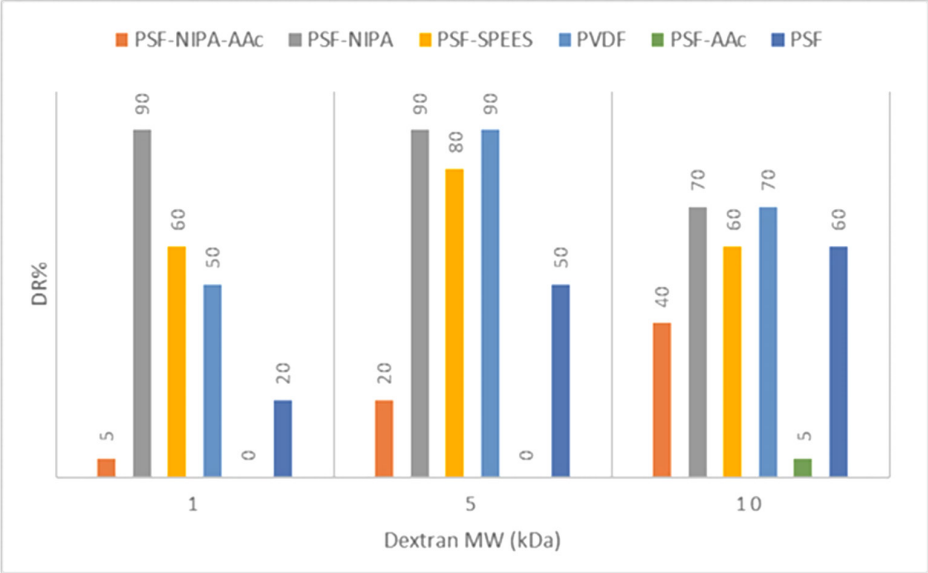

Figure 5. Dextran retention percentage (DR%) and pore size distribution in PSF-SRP membranes and PVDF membrane control.

Experimental determination of the MWCO data indicated a deviation from the theoretical MWCO data (Table 2). The difference was attributed to pressure and flow conditions used in the experimental filtration system.

The dextran rejection study indicated that the SRPs modified the membrane pores of PSF, suggesting narrower pore sizes in PSF-NIPA and PSF-SPEES, but pore extension in PSF-AAc.

Specifically, PSF-SRP membranes, as well as the PSF and PVDF membranes (as control), retained dextran particles at 10 kDa, showing a DR% range of 40–70%, except for PSF-AAc, which retained only 5% of DR.

Dextran 5 kDa was also retained by the PSF-SRP membranes; notably, the highest retention was achieved by PVDF, PSF-NIPA, and PSF-SPEES, followed by PSF and PSF-NIPA-AAc, whereas PSF-AAc did not retain these particles.

In sequence, high dextran retention with 1 kDa molecules was observed in PSF-NIPA, maintaining retention ability up 90%, whereas PVDF, PSF, PSF-SPEES, and PSF-NIPA-AAc presented low capacity of retention of dextran at 1 kDa. Therefore, the predominant pores in PSF-SPEES, PSF-NIPA, PSF-NIPA, and PVDF membranes were in the 1–10 kDa range, and the range of 1–5 kDa was predominant in PSF-NIPA, PSF-SPEES, and PVDF membranes.

Consequently, based on the dextran retention measurements, MWCO of PSF, PSF-SPEES, and PVDF membranes indicate their utility in the ultrafiltration (UF) range of membranes (of 5–10 kDa), due to the predominant pore size of 10 kDa. In turn, PSF-NIPA

was considered to be in the NF range of 1–5 kDa with major pores of 1 kDa, whereas PSF-NIPA-AAc was identified in the MF range, with major pores of 50–100 kDa.

In addition, according to the latest data, the membrane polarization in PSF, PSF-NIPA, PSF-SPEES, and PVDF membranes was predicted by feeding dextran at 10 kDa, according to the MWCO of the membranes and the MW of dextran.

Previous studies have shown that the changes in the pore structure and pore size of the pristine membranes affect their ability to reject molecules. These changes can increase membrane transport; however, in other cases, a negative effect can be observed with the presence of SRPs.

Saini et al. [46] used AAc in the casting solution for fabrication of modified PSF membranes using the phase inversion method, with increases in the porosity, pore density, and permeability when 1.5 wt% of copolymer was used, thus enhancing the retention–permeation effect. Choi et al. [16] modified PES membranes using PDN and utilized proteins as model molecules to analyze the membrane retention behavior, showing that the PES/PDN membrane containing 5% PDN separated three different MW proteins with high efficiency. However, the temperature of the membrane had a great influence on this result, as PDN is a thermo-responsive polymer. In this case, the flux recovery ratio was described as ranging from 29% to 69%.

Beshahwored et al. [44] tested the inclusion of polybenzimidazole (PBI) into sulfonated polyphenylsulfone (sPPSU) for herbicide removal and drug separation in the context of organic solvent nanofiltration (OSN). The membrane PBI-sPPSU exhibited smaller pore size and pore size distribution, as well as better separation performance with >96% rejection against low-molecular-weight pendimethalin from water and tetracycline from ethanol.

In turn, Ghassemi et al. [19] analyzed the rejection rate of BSA through surface modification of PES membrane by grafting with NIPA. They observed a high capacity for BSA rejection due to modification of pore structure in PES, thus impacting the flux recovery ratio of the membranes, as NIPA provided a hydration layer which reduced the interaction between BSA and the membrane surface. Furthermore, BSA fouling was easily removed from the grafted PES membranes when the cleaning temperature was increased.

2. Water flux of PSF-SRP membranes. Figure 6 shows membrane water flux Jp (mL/scm^2) of the PSF-SRP membranes and PVDF membrane (control) under different operating conditions. The data correspond to (a) variation in TMP (2–8 bar) with feeding of distilled water at room temperature (20 °C) and pH 6.6; (b) feed temperature variation (20–40 °C) with feeding of distilled water at pH 6.6 and TMP of 7–8 bar; and (c) feed pH ranging from 4 to 8 at room temperature (20 °C) with TMP of 7–8 bar. The results for PSF-AAc membranes are not included here, as the obtained data were inconsistent, which was related to the characteristics of pore radius, porosity, MWCO, mechanical resistance, and swelling degree.

According to TMP, feed temperature, and feed pH variations, the Jp fluxes for PSF-SRP membranes showed different behaviors. The PVDF membrane exhibited the lowest Jp, as it is a hydrophobic membrane. Subsequently, the flux of PSF was higher than that of PVDF; moreover, the fluxes of PSF-SRP exceeded that of the PSF membrane, as PSF is a hydrophilic material and the presence of SRPs increased the anti-fouling properties of PSF [47–50].

Sequentially, the Jp of PSF-SRP membranes under TMP variations showed typical behavior, with Jp values increasing with TMP; however, each membrane presented different Jp fluxes. PSF-NIPA-AAc showed the highest Jp values (2.5–3.5 mL/scm^2), as its MWCO corresponds to the MF range; however, the maximum TMP result was observed at 4 bar. In turn, PSF, PSF-SPEES, and PVDF displayed less Jp (1–2 mL/scm^2), as their MWCO was in the UF range, observing a maximum at TMP of 5 bar, whereas PSF-NIPA did not present permeation under TMP of 2–5 bar. Instead, water flux was detected at 6–8 bar, due to its NF range of filtration, with a maximum at TMP of 7 bar.

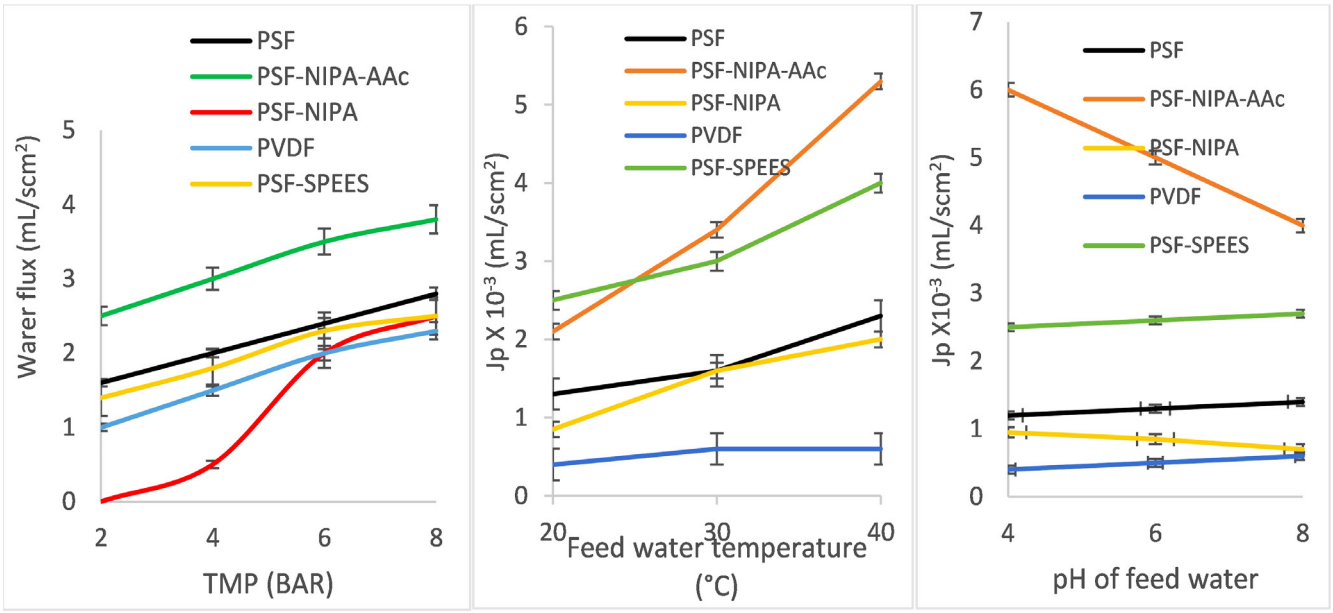

(**a**) (**b**) (**c**)

Figure 6. Water fluxes (Jp, mL/scm^2) of PSF-SRP membranes (including PVDF membrane) under different operating conditions: (**a**) TMP range 2–8 bar; (**b**) feed temperature range 20–40 °C; and (**c**) feed pH range 4–8.

Furthermore, the water fluxes Jp of PSF-SRP membranes increased with increasing feed temperature (20–40 °C); however, the PVDF membrane control did not show observable change with feed temperature. PSF-SPEES and PSF-NIPA displayed notorious Jp increments when the feed temperature increased, suggesting a positive effect due to presence of SPEES and NIPA in PSF, as the MWCO of PSF-SPEES and PSF-NIPA was lower than that of PSF, suggesting that the Jp was increased due to temperature stimuli. Zhu et al. [44] reported a similar behavior for NIPA-grafted PES membranes, showing a sudden flux increase when they reached 32–40 °C.

In turn, the Jp behavior of PSF-SRP membranes under pH variations suggested the influence of the SRPs in the PSF membranes. Particularly, PSF-SPEES showed a constant behavior in relation to the pH, suggesting that SPEES provided stimuli-responsive properties in PSF, including a change in pore size and enhanced transport properties [8].

Furthermore, PSF-NIPA-AAc showed the highest Jp values; however, this performance was observed at acidic pH, whereas, under basic conditions, the Jp was decreased. This result was associated with the presence of AAc as, at basic pH, AAc produces a high charge density of carboxyl groups, reducing the membrane pore size and, consequently, the water flux.

The dependence of AAc on the pH has been reported by Zhu et al. [50], who confirmed that AAc increases the membrane hydrophilicity and positively alters membrane permeation. Luo et al. [33] also reported the change of water flux in PES membranes due to the presence of AAc. The authors observed that, at acidic pH, the membrane fluxes were high, whereas, at pH > 4, the flux was low. This is because, at acidic pH, the protonation of carboxyl groups of AAc led to the opening of the pores of the membrane, causing high fluxes. In contrast, at neutral or weak alkaline pH, the carboxyl groups of the AAc chains are dissociated and negatively charged, producing small fluxes.

With pH variation, NIPA also produced water flux changes in PSF. At basic pH, NIPA showed a low water flux. The result was associated with the presence of hydrophobic groups from NIPA and pore structure modification in the PSF membrane. The stimuli response of NIPA has been previously reported by Zhu et al. [36], who demonstrated that NIPA produces double-responsive pore size and separation ability in PSF, as it is a

thermo-responsive polymer. At basic pH or low temperature, the membrane surfaces and pore walls swell, leading to a small pore size, low water permeability, and low MWCO. On the contrary, when the solution pH is acidic or the temperature is higher, NIPA produces a large pore size, and an increase in water permeability can be observed in the membrane.

Ghassemi et al. [19] recently showed that NIPA has a great influence on the membrane flux. The authors grafted NIPA onto the surface of a PES membrane, enhancing the flux by 13% and enabling a 26% increase in the flux recovery ratio. Furthermore, an important rejection and antifouling ability was achieved, with a >98% rejection rate for both oil–water emulsion and BSA being reported.

Additionally, SPEES has been reported as a good material for the manufacture of SRP-blended membranes in terms of enhancing the water flux in ion exchange membranes, as the ionic nature of SPEES allows for increased conductivity; however, there are scarce data on its behavior in other types of separation membranes.

Khan et al. [45] used SPEES blended with carbon nanotubes to produce a hydrophilic ion exchange membrane. The property was associated with high concentrations of sulfonic acid groups.

3. Salt rejection and fouling analysis of PSF-SRP membranes. Figure 7a presents the salt rejection ability of PSF-SRP and PVDF membranes during the treatment of a saline industrial effluent containing 10,000–20,000 mg/L TDS equivalent to salts. Figure 7b indicates the membrane resistances, including resistances due to fouling (HFR), reversible fouling (RFR), and irreversible fouling (IFR). The data correspond to membrane operating conditions of 8 bar of TMP and room temperature.

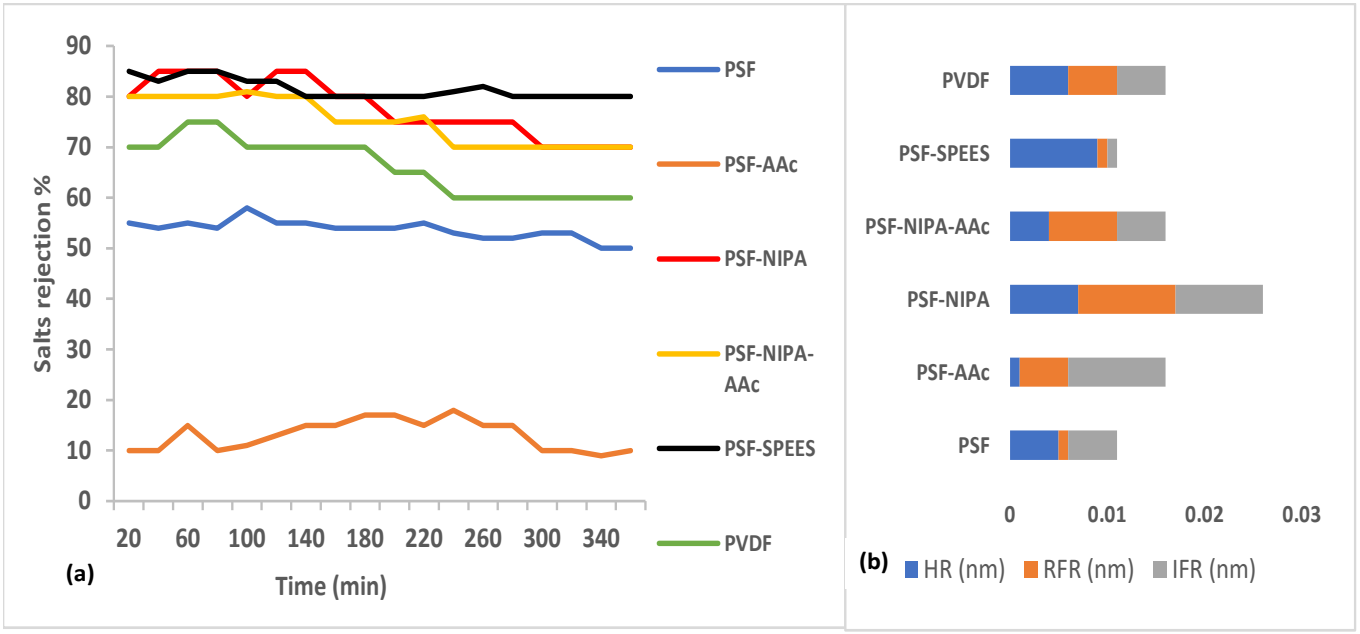

Figure 7. (**a**) Rejection percentage of salts from PSF-SRP and PVDF membranes during the treatment of a saline industrial effluent containing 10,000–20,000 mg/L of total solids (TS) at 25 °C, pH 9, and 8 bar of TMP; (**b**) membrane resistance (nm), including HR, RFR, and IFR.

In general, the incorporation of SRPs in PSF increased the salt rejection percentage of the PSF-SRP membranes.

The PVDF and PSF membranes showed salt rejection ranges of 70–80% and 60–70%, respectively, whereas PSF-NIPA, PSF-NIPA-AAc, and PSF-SPEES obtained 70–90% salt rejection, thus enhancing this property by 10–20% with respect to PSF and PVDF. However, PSF-AAc was the exception, showing reduced salt rejection (10–20%) due to the formation of channels in PSF with the addition of AAc, thus hindering the retention of salts.

The salt rejection enhancement in PSF-SRP membranes was attributed to the pore size reduction in the membranes and the presence of hydrophilic polymers NIPA, AAc, and SPEES, thus increasing the hydrophilicity and salt rejection ability of the membranes.

Similar experiments under different pH (range: 4–8) demonstrated that the highest salt rejection percentage for PSF-NIPA, PSF-SPEES, and PSF-NIPA-AAc membranes was observed at pH 8; meanwhile, PSF-AAc, PVDF, and PSF maintained a similar behavior, showing the lowest salt rejection at pH 4.

The increase in salt rejection by PSF-SRP membranes was linked to the presence of SPEES, NIPA, and AAc, given that they act as pH-responsive materials.

Sequentially, Figure 7b shows hydraulic membrane resistance (HR) and reversible (RFR) and irreversible fouling resistance (IFR) data for the PSF-SRP membranes.

As a result, it can be concluded that the presence of SRPs in the PSF membrane modified the original resistance behavior, leading to different values of HR, RFR, and IFR.

The lowest HR was observed in PSF-AAc and PSF-NIPA-AAc membranes, indicating high water transport due to the presence of AAc. In this case, it can be suggested that AAc reduced the original resistance of PSF. On the contrary, the highest HR was observed in PSF-SPEES; therefore, SPESS increased the HR in PSF.

The incidence of SRP in PSF membranes also changed the RFR and IFR performances. The highest predisposition to membrane saturation was observed in PSF-SPEES and PSF, in accordance with the lowest FRR and IFR, whereas PSF-NIPA presented a balance between HR, FRR, and IFR, suggesting an equilibrated resistance behavior.

The capacity of AAc as an antifouling polymer in membranes has been reported in several previous studies. Saini et al. [7] used AAc to modify PSF membranes, increasing the fouling resistance to BSA molecules. Borzęcka et al. [6] modified the surface of polypropylene (PP) membranes with AAc using a grafting process. As a result, they observed that the presence of AAc on the membrane surface may decrease fouling, due to the mass of silica particles deposited on the membrane surface. Principally, this tendency was visible at a pH of 10, which was confirmed through simulation of the repulsive force between brushes and foulant particles.

In a similar context, Saini et al. [51] synthesized an antifouling PVDF membrane through incorporating an amphiphilic copolymer, namely poly(vinylidene fluoride)-graft-Poly(2-N-morpholino)ethyl methacrylate (PVDF-g-PMEMA). The presence of PMEMA produced thermo- and pH-responsive properties and improved the antifouling characteristics of the PVDF membrane, avoiding fouling during the treatment of oil wastewater.

Seah et al. [52] fabricated a thin film nanocomposite membrane using graphene oxide and AAc for the treatment of textile wastewater, resulting in a 25% enhancement of pigment retention and high saline permeation, allowing for its reuse.

4. Conclusions

PSF, PSF-SPEES, PSF-NIPA, PSF-AAc, and PSF-NIPA-AAc membranes were synthesized to produce responsive PSF-SRP membranes with high salt rejection response and water permeation, thus allowing for the desalination and purification of effluents derived from the food industry. In addition, a PVDF membrane was utilized as a control membrane for comparison, considering its thermal and mechanical resistance, as well as its hydrophobic characteristics.

The incorporation of SRPs in PSF altered the original membrane's structure, porosity, and performance. The principal results were observed in terms of the surface characteristics, porosity, MWCO, thermal and mechanical responses, and membrane performance.

PSF-SPEES and PSF-NIPA showed homogeneous structures and increased porosity in comparison with PSF. In turn, their pore radii were decreased, placing them in the UF–NF membrane range, with a high proportion of 1–10 kDa pores. Furthermore, PSF-NIPA was placed in the NF range, with a majority of pores at 1 kDa, whereas SPF-SPEES was placed in the UF range, with a similar predominance of pores to PSF (10 kDa). Meanwhile, a more drastic change was observed in the presence of AAc; PSF-NIPA-AAc was placed in the MF

range, with prevailing pores of 100 kDa, whereas PSF-AAc resulted in an asymmetrical structure, showing the formation of canals and minimal pores. The dextran retention tests also indicated the null retention and low pore predominance of the latter.

The analysis of the membrane performance of the PSF-SRP membranes indicated that PSF-NIPA and PSF-NIPA-AAc gained thermo-responsive properties, increasing the water flux by 60% with respect to PSF, which was maintained in the temperature range of 20–40 °C; meanwhile, the behavior of PSF-SPEES was similar to that of PSF. Therefore, SPEES did not alter the thermic behavior of PSF.

In turn, PSF-NIPA and PSF-SPEES provided pH-responsive properties, showing a similar water flux behavior in the pH range of 4–8. However, PSF-NIPA-AAc drastically reduced the water flux at pH 8.

Regarding the applicability of the membranes, PSF-SPEES and PSF-NIPA presented high desalination responses, enhancing the salt rejection ability by 30–40% with respect to PSF.

The antifouling characteristics of the PSF membranes were also enhanced; the highest resistance to reversible and irreversible fouling was presented by PSF-NIPA, whereas PSF-SPEES showed high hydraulic resistance, but low resistance to reversible and irreversible fouling during the desalination of industrial effluent.

As an important observation, the PSF-SRP membranes showed higher fluxes than the PSF and PVDF (control) membranes, indicating that the SRPs provided an important enhancement in comparison with commercial membranes manufactured using PSF or PVDF.

The obtained data contribute to the literature on the synthesis and application of membranes in sustainable processes involving the desalination of industrial effluents for water recovery and reuse, thus providing environmental and economic benefits.

Author Contributions: Conceptualization, E.V. and C.M.; Methodology, C.M. and S.P.-S.; Validation and Formal analysis, Y.A., V.D.-B. and C.M.; Investigation, E.V. and K.H.; Resources, C.M. and S.P.-S.; Writing—original draft preparation, E.V.; Writing—review and editing, C.M. and S.P.-S.; Project administration, K.H.; Funding acquisition, C.M. and S.P.-S. All authors have read and agreed to the published version of the manuscript.

Funding: This research was funded by Tecnológico Nacional de México (TECNM) projects 17371.23-P.

Institutional Review Board Statement: Not applicable.

Informed Consent Statement: Not applicable.

Data Availability Statement: Data available on application to the authors.

Acknowledgments: The authors thank Tecnológico Nacional de México/Instituto Tecnológico de Tijuana for providing its facilities to develop this study.

Conflicts of Interest: The authors declare no conflicts of interest.

References

1. Gugliuzza, A.; Basile, A. Membrane processes for biofuel separation: An introduction. In *Membranes for Clean and Renewable Power Applications*; Woodhead Publishing: Sawston, UK, 2014; pp. 65–103. [CrossRef]
2. Shen, J.; Liu, G.; Huang, K.; Jin, W.; Lee, K.R.; Xu, N. Membranes with fast and selective gas-transport channels of laminar graphene oxide for efficient CO_2 capture. *Chem. Soc. Rev.* **2015**, *127*, 588–592. [CrossRef]
3. Vázquez, E.; Muro, C.; Illescas, J.; Burillo, G.; Hernández, O.; Rivera, E. Obtainment and Characterization of Hydrophilic Polysulfone Membranes by N-Vinylimidazole Grafting Induced by Gamma Irradiation. *Polymers* **2020**, *12*, 1284. [CrossRef] [PubMed]
4. Vázquez-Fernández, I.; Bouzina, A.; Raghibi, M.; Timperman, L.; Bigarré, J.; Anouti, M. Influence of hydrophilic/hydrophobic protic ionic liquids (PILs) on the poly (vinylidene fluoride)(PVDF-ionic liquid) membrane properties. *J. Mater. Sci.* **2020**, *55*, 16697–16717. [CrossRef]

5. Chaudhuri, A.; Sandha, K.K.; Agrawal, A.K.; Gupta, P.M. Introduction to smart polymers and their application. Smart Polymeric Nano-Constructs. In *Drug Delivery*; Academic Press: Oxford, UK, 2023; pp. 1–46. [CrossRef]
6. Borzęcka, N.H.; Kozłowska, I.; Gac, J.M.; Bojarska, M. Anti-fouling properties of poly (acrylic acid) grafted ultrafiltration membranes–experimental and theoretical study. *Appl. Surf. Sci.* **2020**, *506*, 144658. [CrossRef]
7. Saini, B.; Sinha, M.K.; Dey, A. Functionalized polymeric smart membrane for remediation of emerging environmental contaminants from industrial sources: Synthesis, characterization and potential applications. *Process. Saf. Environ.* **2022**, *161*, 684–702. [CrossRef]
8. Hou, J.; Sutrisna, P.D.; Zhang, Y.; Chen, V. Formation of ultrathin, continuous metal–organic framework membranes on flexible polymer substrates. *Chem. Int. Ed.* **2016**, *55*, 3947–3951. [CrossRef]
9. Al-Najar, B.; AlBuflasa, H.; Naushad, M. Smart polymer coatings for membrane antifouling applications. In *Smart Polymer Nanocomposites*; Woodhead Publishing: Sawston, UK, 2021; pp. 415–450. [CrossRef]
10. Vanangamudi, A.; Dumée, L.F.; Des Ligneris, E.; Duke, M.; Yang, X. Thermo-responsive nanofibrous composite membranes for efficient self-cleaning of protein foulants. *J. Membr. Sci.* **2019**, *574*, 309–317. [CrossRef]
11. Guclu, S.; Kizildag, N.; Dizman, B.; Unal, S. Solvent-based recovery of high purity polysulfone and polyester from end-of-life reverse osmosis membranes. *SM&T* **2022**, *31*, e00358. [CrossRef]
12. He, H.; Liu, Y.; Wang, L.; Qiu, W.; Li, D.; Liu, Z.; Ma, J. Improvements of ferrate (VI) pretreatment on membrane flux and membrane rejection using cheap NaClO reagent. *Water. Res.* **2023**, *229*, 119520. [CrossRef]
13. Hai, A.; Rambabu, K.; Govindan, B.; Banat, F.; Naushad, M. Smart polymeric composite membranes for wastewater treatment. In *Smart Polymer Nanocomposites*; Woodhead Publishing: Sawston, UK, 2021; pp. 313–350. [CrossRef]
14. Warsinger, D.M.; Chakraborty, S.; Tow, E.W.; Plumlee, M.H.; Bellona, C.; Loutatidou, S.; Karimi, L.; Mikelonis, A.M.; Achilli, A.; Ghassemi, A.; et al. A review of polymeric membranes and processes for potable water reuse. *J. Org. Chem.* **2018**, *8*, 209–237. [CrossRef]
15. Musarurwa, H.; Tavengwa, N.T. Stimuli-responsive polymers and their applications in separation science. *React. Funct. Polym.* **2022**, *175*, 105282. [CrossRef]
16. Choi, J.Y.; Yun, T.; Kwak, S.Y. Two-step thermoresponsive membrane with tunable separation properties and improved cleaning efficiency. *J. Membr. Sci* **2018**, *554*, 117–124. [CrossRef]
17. Liu, M.; Yu, C.; Dong, Z.; Jiang, P.; Lü, Z.; Yu, S.; Gao, C. Improved separation performance and durability of polyamide reverse osmosis membrane in tertiary treatment of textile effluent through grafting monomethoxy-poly (ethylene glycol) brushes. *Sep. Purif. Technol.* **2019**, *209*, 443–451. [CrossRef]
18. Chen, F.F.; Su, T.; Zhao, X.T.; Pan, J.F.; Liu, L.F. A rigid-flexible interpenetrating polyamide reverse osmosis membrane with improved antifouling property fabricated via two step modifications. *J. Membr. Sci.* **2021**, *637*, 119625. [CrossRef]
19. Ghasemi, H.; Abu-Zahra, N.; Baig, N.; Abdulazeez, I.; Aljundi, I.H. Enhancing fouling resistance and separation performance of polyethersulfone membrane through surface grafting with copolymerized thermo-responsive polymer and copper oxide nanoparticles. *Chem. Eng. J. Adv.* **2023**, *16*, 100528. [CrossRef]
20. Hu, Q.; Zhou, F.; Lu, H.; Li, N.; Peng, B.; Yu, H.; Yuan, Y.; Zhang, H. Improved antifouling performance of a polyamide composite reverse osmosis membrane by surface grafting of dialdehyde carboxymethyl cellulose (DACMC). *J. Membr. Sci.* **2021**, *620*, 118843. [CrossRef]
21. Lü, Z.; Guo, Z.; Zhang, K.; Yu, S.; Liu, M.; Gao, C. Separation and anti-dye-deposition properties of polyamide thin-film composite membrane modified via surface tertiary amination followed by zwitterionic functionalization. *J. Membr. Sci.* **2020**, *604*, 118063. [CrossRef]
22. Li, Z.; Xu, Y.; Shen, L.; Li, R.; Jiao, Y.; Lin, H.; Tang, C.Y. Nano-wrinkled polyamide membrane preparation via heterogeneous surface-regulated interfacial polymerization for enhanced desalination performance. *Desalination* **2023**, *564*, 116801. [CrossRef]
23. Zhao, D.L.; Yeung, W.S.; Zhao, Q.; Chung, T.S. Thin-film nanocomposite membranes incorporated with UiO-66-NH2 nanoparticles for brackish water and seawater desalination. *J. Membr. Sci.* **2020**, *604*, 118039. [CrossRef]
24. Zhu, L.J.; Song, H.M.; Li, C.; Wang, G.; Zeng, Z.X.; Xue, Q.J. Surface wormlike morphology control of polysulfone/poly (N-isopropylacrylamide) membranes by tuning the two-stage phase separation and their thermo-responsive permselectivity. *J. Membr. Sci.* **2018**, *555*, 290–298. [CrossRef]
25. *ASTM D2578-04*; Standard Test Method for Wetting Tension of Polyethylene and Polypropylene Films. ASTM International: Conshohocken, PA, USA, 2004.
26. *ASTM C 813-90*; Standard Test Method for Hydrophobic Contamination on Glass by Contact Angle Measurement. ASTM International: Conshohocken, PA, USA, 1990.
27. *ASTM D 5946-99*; Standard Test Method for Corona-Treated Polymer Films Using Water Contact Angle Measurements. ASTM International: Conshohocken, PA, USA, 1999.
28. Yehl, C.J.; Zydney, A.L. Characterization of dextran transport and molecular weight cutoff (MWCO) of large pore size hollow fiber ultrafiltration membranes. *J. Membr. Sci.* **2021**, *622*, 119025. [CrossRef]

29. Hernández, K.; Muro, C.; Ortega, R.E.; Velazquez, S.; Riera, F. Water recovery by treatment of food industry wastewater using membrane processes. *Environ. Technol.* **2021**, *42*, 775–788. [CrossRef]
30. Zaragoza, S.; Muro, C.; Hernández, K.; Díaz-Blancas, V.; Sonia Martínez, M.; Francisco, R. Separation and phenol recovery from resin effluents by ultrafiltration. A proposal to use this method on an industrial scale. *Chem. Eng. Commun.* **2023**, *210*, 47–60. [CrossRef]
31. Zhu, L.; Song, H.; Zhang, D.; Wang, G.; Zeng, Z.; Xue, Q. Negatively charged polysulfone membranes with hydrophilicity and antifouling properties based on in situ cross-linked polymerization. *J. Colloid Interface Sci.* **2017**, *498*, 136–143. [CrossRef]
32. Mao, H.; Zhou, S.; Shi, S.; Xue, A.; Li, M.; Cai, J.; Zhao, Y.; Xing, W. Anti-fouling and easy-cleaning PVDF membranes blended with hydrophilic thermo-responsive nanofibers for efficient biological wastewater treatment. *Sep. Purif. Technol.* **2022**, *281*, 119881. [CrossRef]
33. Luo, T.; Lin, S.; Xie, R.; Ju, X.J.; Liu, Z.; Wang, W.; Mou, C.L.; Ahao, C.; Chen, Q.; Chu, L.Y. pH-responsive poly (ether sulfone) composite membranes blended with amphiphilic polystyrene-block-poly (acrylic acid) copolymers. *J. Membr. Sci.* **2014**, *450*, 162–173. [CrossRef]
34. Plisko, T.; Burts, K.; Penkova, A.; Dmitrenko, M.; Kuzminova, A.; Ermakov, S.; Bildyukevich, A. Effect of the Addition of Polyacrylic Acid of Different Molecular Weights to Coagulation Bath on the Structure and Performance of Polysulfone Ultrafiltration Membranes. *Polymers* **2023**, *15*, 1664. [CrossRef]
35. Manohar, M.; Sharma, P.P.; Kim, D. Intercalated poly (2-acrylamido-2-methyl-1-propanesulfonic acid) into sulfonated poly (1, 4-phenylene ether-ether-sulfone) based proton exchange membrane: Improved ionic conductivity. *Molecules* **2020**, *26*, 161. [CrossRef]
36. Zhu, L.; Song, H.; Wang, G.; Zeng, Z.; Xue, Q. Symmetrical polysulfone/poly (acrylic acid) porous membranes with uniform wormlike morphology and pH responsibility: Preparation, characterization and application in water purification. *J. Membr. Sci.* **2018**, *549*, 515–522. [CrossRef]
37. Peng, Y.; Fan, H.; Ge, J.; Wang, S.; Chen, P.; Jiang, Q. The effects of processing conditions on the surface morphology and hydrophobicity of polyvinylidene fluoride membranes prepared via vapor-induced phase separation. *Appl. Surf. Sci.* **2012**, *263*, 737–744. [CrossRef]
38. Harruddin, N.; Saufi, S.M.; Faizal, C.K.M.; Mohammad, A.W. Effect of VIPS fabrication parameters on the removal of acetic acid by supported liquid membrane using a PES–graphene membrane support. *RSC Adv.* **2018**, *8*, 25396–25408. [CrossRef]
39. Junker, M.A.; Regenspurg, J.A.; Valdes Rivera, C.I.; Brinke, E.T.; de Vos, W.M. Effects of feed solution pH on polyelectrolyte multilayer nanofiltration membranes. ACS Appl. *Polym. Mater.* **2023**, *5*, 355–369. [CrossRef]
40. Low, S.Q.; Ng, Q.H. Progress of stimuli responsive membranes in water treatment. In *Advanced Nanomaterials for Membrane Synthesis and Its Applications*; Elsevier: Cheras, Malaysia, 2019; pp. 69–99. [CrossRef]
41. Sulatha, M.S.; Natarajan, U. Molecular dynamics simulations of adsorption of poly (acrylic acid) and poly (methacrylic acid) on dodecyltrimethylammonium chloride micelle in water: Effect of charge density. *J. Phys. Chem.* **2015**, *119*, 12526–12539. [CrossRef]
42. Logan, J. Polyelectrolyte polymers—Types, forms, and function. In *Water-Formed Deposits*; Elsevier: Amsterdam, The Netherlands, 2022; pp. 747–764. [CrossRef]
43. Wang, S.Y.; Gonzales, R.R.; Zhang, P.; Istirokhatun, T.; Takagi, R.; Motoyama, A.; Fang, L.F.; Matsuyama, H. Surface charge control of poly (methyl methacrylate-co-dimethyl aminoethyl methacrylate)-based membrane for improved fouling resistance. *Sep. Purif. Technol.* **2021**, *279*, 119778. [CrossRef]
44. Beshahwored, S.S.; Weber, M.; Hu, C.C.; Lai, J.Y.; Chung, T.S. Effects of sulfonation degree on compatibility and separation performance of polybenzimidazole (PBI)-sulfonated polyphenylenesulfone (sPPSU) blend membranes. *J. Membr. Sci.* **2023**, *683*, 121849. [CrossRef]
45. Khan, A.; Jain, R.K.; Banerjee, P.; Ghosh, B.; Inamuddin; Asiri, A.M. Development, characterization and electromechanical actuation behavior of ionic polymer metal composite actuator based on sulfonated poly (1, 4-phenylene ether-ether-sulfone)/carbon nanotubes. *Sci. Rep.* **2018**, *8*, 9909. [CrossRef]
46. Saini, B.; Khuntia, S.; Sinha, M.K. Incorporation of cross-linked poly (AA-co-ACMO) copolymer with pH responsive and hydrophilic properties to polysulfone ultrafiltration membrane for the mitigation of fouling behaviour. *J. Memb. Sci.* **2018**, *572*, 184–197. [CrossRef]
47. Modi, A.; Bellare, J. Efficiently improved oil/water separation using high flux and superior antifouling polysulfone hollow fiber membranes modified with functionalized carbon nanotubes/graphene oxide nanohybrid. *J. Environ. Chem. Eng.* **2019**, *7*, 102944. [CrossRef]
48. Alkhouzaam, A.; Qiblawey, H. Synergetic effects of dodecylamine-functionalized graphene oxide nanoparticles on antifouling and antibacterial properties of polysulfone ultrafiltration membranes. *J. Water Process. Eng.* **2021**, *42*, 102120. [CrossRef]
49. Mahdavi, H.; Karami, M.; Heidari, A.A. Preparation of mixed matrix membranes made up of polysulfone and MIL-53 (Al) nanoparticles as promising membranes for separation of aqueous dye solutions. *Sep. Purif. Technol.* **2021**, *274*, 119033. [CrossRef]
50. Zhu, G.D.; Yang, C.Y.; Yin, Y.R.; Yi, Z.; Chen, X.H.; Liu, L.F.; Gao, C.J. Preparation of isoporous membranes from low χ block copolymers via co-assembly with H-bond interacting homopolymers. *J. Membr. Sci.* **2019**, *589*, 117255. [CrossRef]

51. Saini, B.; Vaghani, D.; Khuntia, S.; Sinha, M.K.; Patel, A.; Pindoria, R. A novel stimuli-responsive and fouling resistant PVDF ultrafiltration membrane prepared by using amphiphilic copolymer of poly (vinylidene fluoride) and Poly (2-N-morpholino) ethyl methacrylate. *J. Memb. Sci.* **2020**, *603*, 118047. [CrossRef]
52. Seah, M.Q.; Lau, W.J.; Goh, P.S.; Ismail, A.F. Greener synthesis of functionalized-GO incorporated TFN NF membrane for potential recovery of saline water from salt/dye mixed solution. *Desalination* **2022**, *523*, 115403. [CrossRef]